Habib Cherif

Jamel Belhadj

J. Electrical Systems 10-2 (2014): 117-132

Regular paper

Journal of Electrical Systems

Energy output estimation of hybrid Wind-Photovoltaic power system using statistical distributions

In this paper, an estimation of the energy production of stand-alone hybrid wind turbine-photovoltaic system in southern Tunisia is studied. Energy estimation using probability distribution functions is applied. Three different probability density functions were used in this study: Weibull, Beta, and Log-normal. The climatic conditions for Djerba Island (Southern Tunisia) were used. The design of the hybrid system architecture according to all the characteristics of the studied site is presented. Monthly average hybrid energy production is estimated in the DC bus including the global losses and taking into account the stochastic nature of wind speed and solar irradiance. The power loss models involved in the hybrid system converters are investigated. Capacity factors of the wind turbine and photovoltaic station are presented. The obtained results show that the integration of all losses and using the statistical distributions leads to a better energy estimation taking into account all the characteristics of the southern Tunisia site.

Keywords: Hybrid system, Energy estimation, Wind-Photovoltaic energy, Converters losses, Capacity factor, Statistical distributions.

1. Introduction

Today, there are many hybrid systems used for electricity and/or matter (water, hydrogen) production [1]. Basically, hybrid systems combine two or more energy sources from renewable energy technologies and from conventional technologies [2–4]. In fact, to decrease the cost and increase the production of a hybrid system, we need to reduce the relative investment cost, introduce more reliable design methods, and utilize the best available installation sites. However, the studied hybrid system combines two energy sources from renewable energy technologies: wind turbines and solar panels [5,6]. Actually, hybrid wind turbine-photovoltaic source is considered to be an excellent solution compared to stand-alone single source since wind is usually more available in colder months and solar resources during the warmer months [7]. Based on meteorological data, Southern Tunisia has good solar and wind power potentials. Therefore, the use of renewable energy (hybrid system: wind and photovoltaic) in these regions would be of great benefit, especially in remote locations. Hybrid systems can increase electrical energy for private consumers and small business and/or can be used to supply many applications as water pumping and desalination [8,9].

In this context, we focus on a large-scale time evaluation for energy estimation of the stand-alone hybrid wind turbine-photovoltaic system in southern Tunisia (Djerba). The evaluation for the energy production estimation is developed with statistical distribution models and all losses integration [10]. First, we present the hybrid system architecture according to all the characteristics of the site. The climatic conditions (temperature, solar irradiance and the wind speed) for Djerba Island are used. Next, an accurate hybrid energy estimation based on the probabilistic approach is presented. In particular, Weibull, Beta, and Log-normal probability density functions are used. In addition, capacity factors of the wind turbine and photovoltaic station are computed and presented. Finally, the estimated electricity in the DC bus from the hybrid wind-photovoltaic system based on all converters losses, the photovoltaic modules losses and the wind turbine losses is investigated.

University of Tunis El Manar, LSE-ENIT, BP 37 Le Belvédère 1002, Tunis, Tunisia cherif.habib@ieee.org
University of Tunis, ESSTT-DGE, BP 56 Montfleury, 1008, Tunis, Tunisia Jamel.Belhadj@esstt.rnu.tn

2. Hybrid wind-photovoltaic system description and location

The hybrid power generation system consists of a 10 kW wind turbine, 400 m² photovoltaic panels and converters. The DC bus voltage is fixed at 600 V and collects the total energy from the hybrid wind-photovoltaic system. The system configuration is presented in Fig. 1. The hybrid system is located in Djerba Island (South Tunisia). The latter region is situated in Northern hemisphere at **33°9'** North latitude and **10°8'** East longitude [11]. The monthly average metrological data are summarized in Table 1.

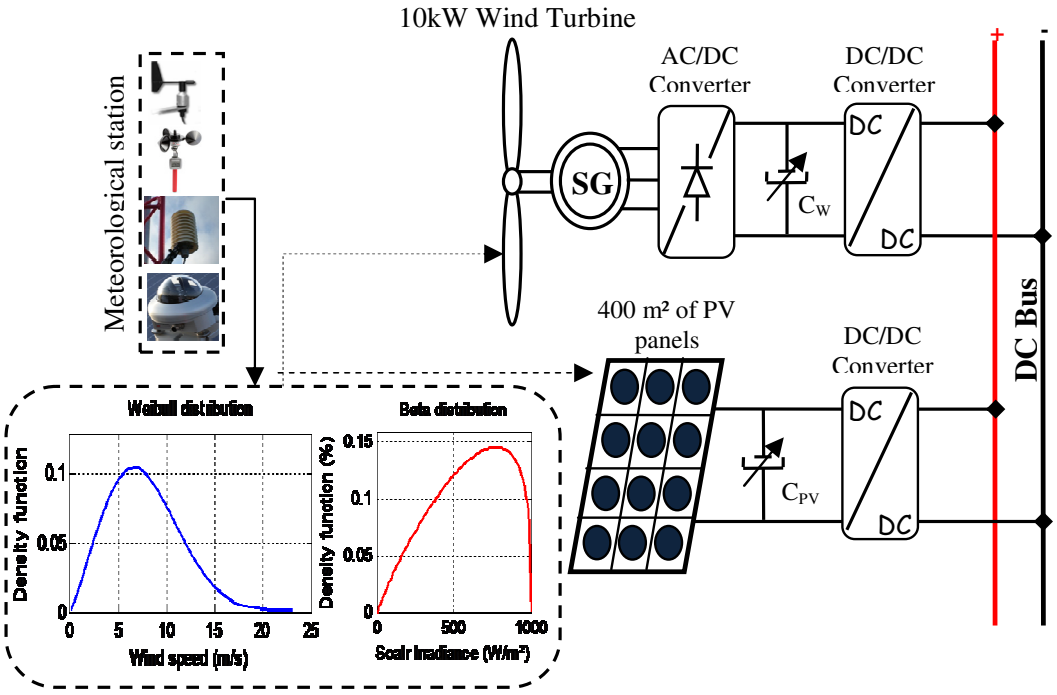

Fig. 1. Hybrid wind turbine-photovoltaic system architecture without battery storage

Table 1: Measured Meteorological Data

Month	Air Temperature (°C)	Daily solar radiation (kWh/m²/d)	Wind speed (m/s)
January	12.9	2.47	7.9
February	13.4	3.58	8.0
March	15.7	4.79	8.3
April	18.0	6.18	8.4
May	21.6	6.93	8.4
June	25.1	7.55	8.4
July	27.6	7.72	7.8
August	28.6	7.09	7.6
September	26.9	5.41	7.9
October	23.3	3.80	7.6
November	18.5	2.64	7.8
December	14.3	2.22	8.4
Annual average	20.5	5.04	8.0

3. Wind energy output estimation model

3.1 Wind energy conversion subsystem

The wind subsystem is composed of a 10 kW wind turbine interconnected to a DC bus through (AC/DC) converter and (DC/DC) converter. The three-phase output of the Permanent Magnet Synchronous Generator (PMSG) are rectified with a diode bridge rectifier and controlled by a (DC/DC) boost converter [11]. Fig. 2 shows the scheme of the wind turbine architecture with a 600 DC bus voltage.

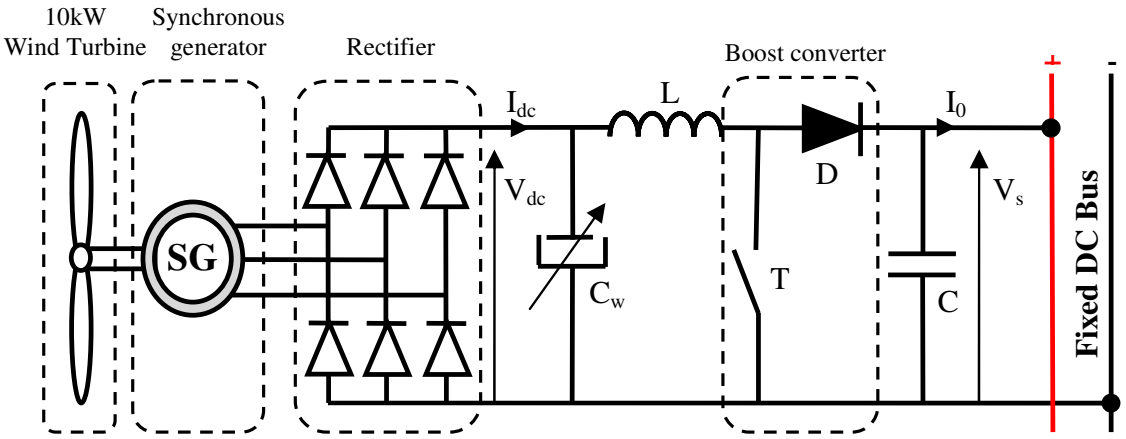

Fig. 2. Wind turbine architecture with a diode bridge rectifier and a (DC/DC) boost converter

3.2 Wind turbine power

The Wind Turbine (WT) type is a direct drive based on a Synchronous Generator (SG). The electrical output power of the wind turbine is given by

$$P_e = 0.5 \cdot \rho \cdot S \cdot V^3 \cdot C_p \cdot \eta \quad (1)$$

where V is the average wind speed (m/s), ρ is the air density (kg/m^3), S is the swept area (m²), C_p is the power coefficient and η is the generator efficiency (%).

The wind turbine is characterized by a starting speed of 3.4 m/s and a rated speed of 13 m/s. The wind turbine characteristics are: Rotor diameter = 7m, Swept area = 38.48 m², Power coefficient = 0.25 and Generator efficiency = 80 %. Fig. 3 shows the open loop electric wind power curve giving by manufacturer's data sheet. At hub height 18.3 m and using Eq. (1), the estimated monthly average electrical output power is given in Fig. 4. We note that the monthly average electrical power production is about 2.5 kW. To estimate the energy production of the selected wind turbine, a probabilistic approach will be used.

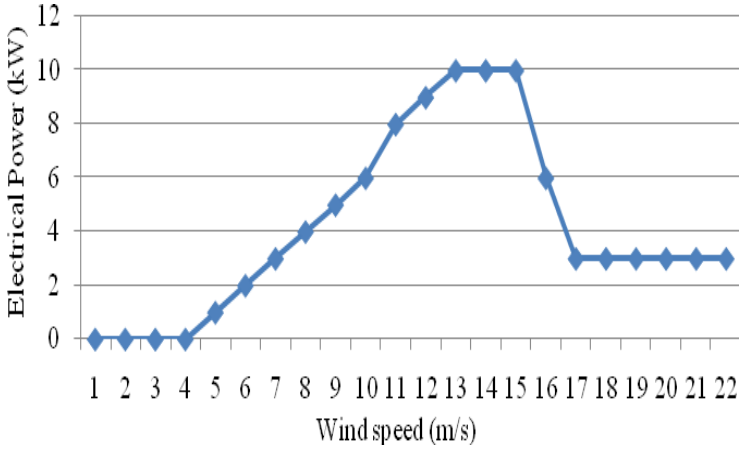

Fig. 3. Power curve of the wind turbine (Bergey BWC Exe)

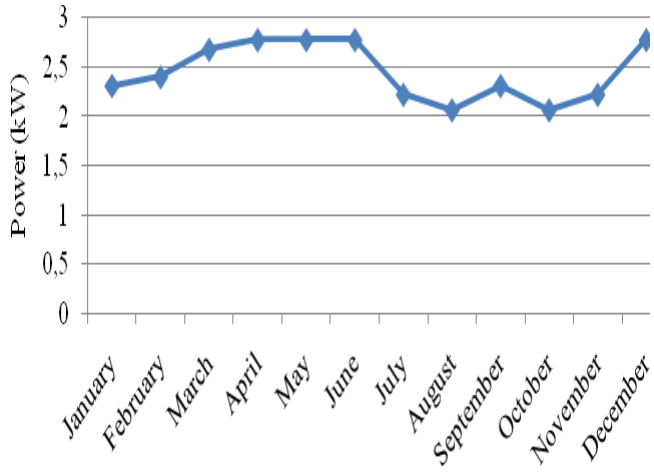

Fig. 4. Produced electrical power by the selected wind turbine

3.3 Wind speed probability density functions

Probability Density Functions (PDFs) are used to describe random variations of the wind speed and to compute the energy production by the used wind turbine. To fit the wind speed at a particular location, different probability density functions such as Weibull, Rayleigh, Rice and Lognormal were used [12,13]. In fact, the most common PDF used for energy production estimation by the selected wind turbine is the Weibull distribution [14,15]. For estimating the two parameters of the Weibull distribution, we use the Least Squares Method (linear regression model). The probability density function is given by

$$f(v)=\frac{k}{c}\left(\frac{v}{c}\right)^{k-1}\exp\left\{-\left(\frac{v}{c}\right)^{k}\right\} \tag{2}$$

where v is the wind speed, k is the shape factor and c is the scale parameter.

Based on the observed occurrence frequencies f_i, the cumulated frequencies F_i of the Weibull distribution are given by

$$F_i = F_{i-1} + f_i \tag{3}$$

Hence, the two parameters of the Weibull distribution are k=2.20 and c=8.70. The cumulative frequencies of the wind speed are given in Fig. 5. Fig. 6 shows the applied simple linear regression model. Fig. 7 shows the probability density curve of the Weibull distribution superimposed with the observed occurrence frequencies of the studied site. The average power from the wind turbine is the power produced at each wind speed multiplied by the Weibull PDF of the wind speed. The estimated monthly average electricity produced by the selected wind turbine using Weibull PDF is given in Fig. 8.

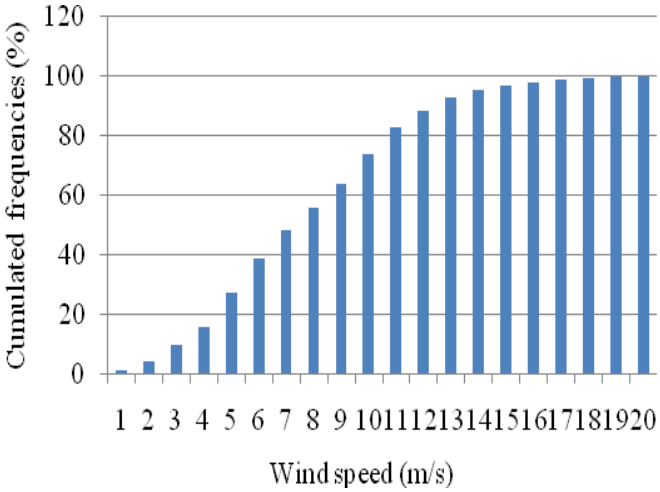

Fig. 5. Cumulative frequencies

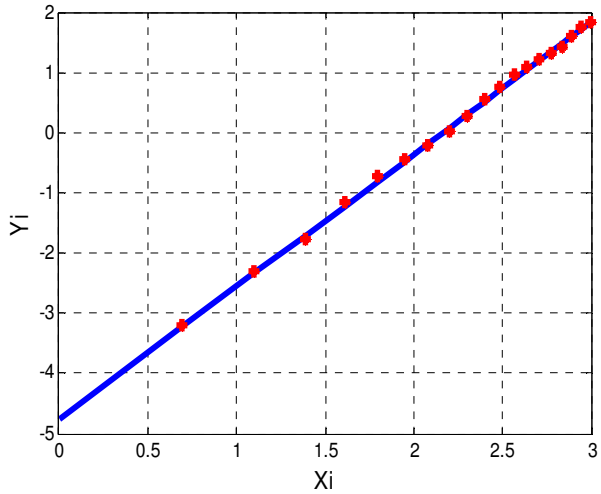

Fig. 6. Simple linear regression

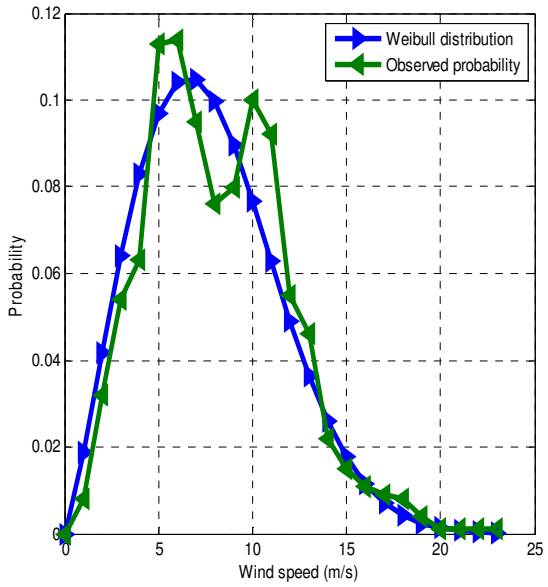

Fig. 7. Weibull and observed distributions

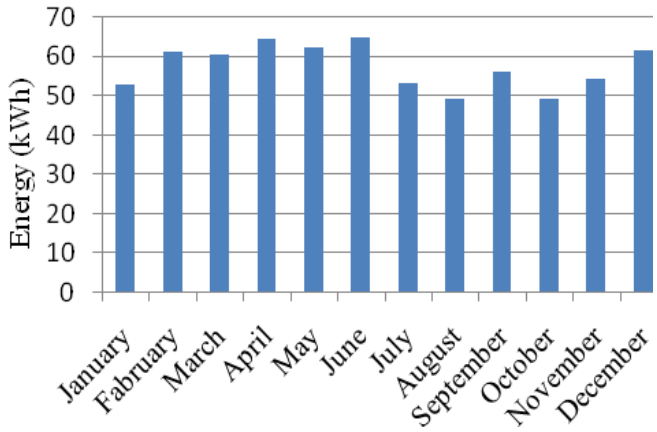

Fig. 8. Monthly average estimated energy from the wind turbine

We note here that the monthly average energy production from the wind turbine is 57.8 kWh and the annual energy production is around 21.01 MWh.

3.4 Converters losses models

For estimated electricity at the DC bus, it is necessary to introduce the converters losses [16]. The variable voltage of the PMSG is converted to DC using uncontrolled diode bridge rectifier. A boost converter is used to match the variable DC voltage with the DC bus voltage [17]. Fig. 2 shows the scheme of the wind turbine architecture. To evaluate the converters losses of the wind subsystem, we compute the conduction and switching losses involved in the boost chopper and the diode bridge rectifier.

3.4.1 Diode rectifier losses

The average conduction power loss is defined as

$$P_{rec\_cond} = 6\left(V_{d0} + r_d \cdot I_{dc}\right) \cdot I_{dc} \tag{4}$$

where I_{dc} is the average rectifier current and V_{dc} is the average rectifier voltage, are given as

$$I_{dc} = \frac{\pi}{\sqrt{6}} \cdot I \tag{5}$$

$$V_{dc} = \frac{3\sqrt{6}}{\pi} \cdot V_{SG} \tag{6}$$

where V_{SG} and I are the RMS values of the PMSG output voltage and current, respectively. Using the typical diode voltage/current graph, the diode voltage drop is approximated by

$$U_d = V_{d0} + r_d \cdot I_{dc} \tag{7}$$

where V_{dO} is the threshold voltage and r_d is the dynamic resistance of the diode.
In this condition, the estimated conduction losses of the rectifier diode are given in Table 2.

3.4.2 Boost converter losses

A. Switching loss

Switching loss includes IGBT (T) turn-on loss and turn off loss. The total IGBT turn-on loss can be defined as

$$W_{on} = \frac{U_T^{ref} \cdot (I_{on} + I_{rr}) \cdot (t_{r\_i} + t_{rr})}{2} \tag{8}$$

where I_{on} is the turn-on current, I_{rr} is the peak reverse recovery current of the diode (free-wheeling diode), t_{r_i} is the current increase time, t_{rr} is the reverse recovery time of the diode, U_T^{ref} is the IGBT voltage reference.

The total IGBT turn-off loss can be calculated by

$$W_{off} = \frac{U_T^{ref} \cdot I_{off} \cdot t_{f\_i}}{2} \tag{9}$$

where I_{off} is the turn-off current and t_{f_i} is the turn-off time. t_{r_i}, t_{rr} and t_{f_i} parameters are depend on the properties of the IGBT giving by manufacturer's data sheet.

The average total IGBT switching losses (on+off) are given by

$$P_{IGBT\_sw} = (W_{on} + W_{off}) \cdot f_s \tag{10}$$

where f_s is the switching frequency. The IGBT switching loss data is given in Table 3.

Table 2: Conduction losses of the diode rectifier

Parameters	Values
V_{d0}	0.8 V
r_d	20 m Ω
I_{dc}	23.68 A
V_{dc}	421.81 V
I	18.48 A
V_{SG}	180.31 V
P_{rec_cond}	181 W

Table 3: IGBT switching losses (on+off) of the boost converter

Parameters	Values
U_T^{ref}	421.81 V
I_{on}	16.6 A
t_{r_i}	$1.14 \cdot 10^{-7}$ s
t_{rr}	$120 \cdot 10^{-9}$ s
I_{off}	16.6 A
t_{f_i}	$1.63 \cdot 10^{-7}$ s
f_s	10 kHz
W_{on}	$11 \cdot 10^{-4}$ J
W_{off}	$5.71 \cdot 10^{-4}$ J
P_{IGBT_sw}	17 W

B. Conduction loss

Using the typical IGBT voltage-current graph, the IGBT voltage drop is given by

$$V_{CE} = U_{CE(sat)} + R_d \cdot I_c \tag{11}$$

where $U_{CE(sat)}$ is the threshold voltage and R_d is the dynamic resistance of the IGBT.

Using the typical diode voltage/current graph, the diode voltage drop is approximated by

$$V_F = U_{d0} + R_{d0} \cdot I_0 \tag{12}$$

where U_{dO} is the threshold voltage and R_{dO} is the dynamic resistance of the diode. $U_{CE(sat)}$, R_d, U_{dO} and R_{dO} can be determined by static characteristics of the IGBT and the diode available from manufacturer's data sheets.

Finally, the average conduction power loss of the IGBT and the diode can be expressed respectively as

$$P_{IGBT\_cond} = V_{CE} \cdot I_c \cdot d \tag{13}$$

$$P_{diode\_cond} = V_F \cdot I_0 \cdot (1-d) \tag{14}$$

where d is the duty cycle. The conduction losses of the boost converter are computed and tabulated in Table 4.

The estimated total power loss of the studied converters (AC/DC and DC/DC) of the proposed wind turbine is 227 W. We present in Fig. 9 the estimated electrical energy in the fixed DC bus with and without converters losses. In the DC-bus, the estimated energy is decreased by nearly 10 % compared to estimated energy without converters losses. It's shown that the loss models of the boost converter and the diode rectifier are significant for accurate energy estimation of the used wind turbine. The Weibull distribution showed an excellent fit for wind energy estimation.

Table 4: IGBT and diode conduction losses of the boost converter

Parameters	Values
$U_{CE(sat)}$	2.3 V
R_d	17.5 m Ω
U_{dO}	1.1 V
R_{dO}	15 m Ω
I_o	16.6 A
P_{IGBT_cond}	13 W
P_{diode_cond}	15.7 W

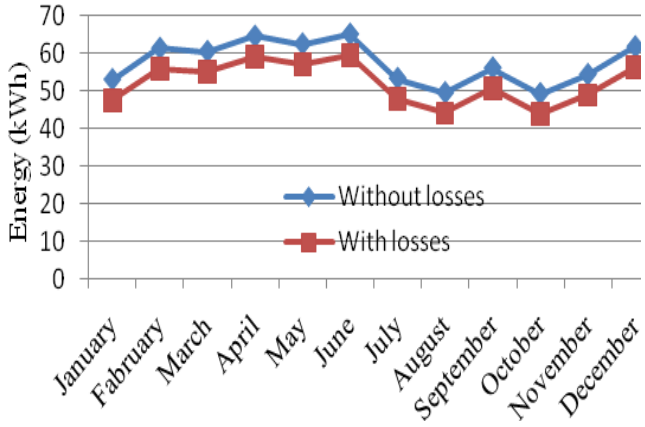

Fig. 9. Monthly average estimated energy in the DC-bus with and without converters losses

3.5 Estimated capacity factor of the wind turbine

Capacity Factor (CF) is defined as the ratio between the total amount of energy produced during a period of time and the energy production it would have produced at full capacity [18]. The capacity factor of the considered wind turbine is calculated at hub height 18.3 m and using Fig. 9 (estimated energy with losses integration). The monthly average capacity factor is given in Fig. 10. We note here that the monthly average wind capacity factor is around 0.24 and 0.18 respectively for June and August.

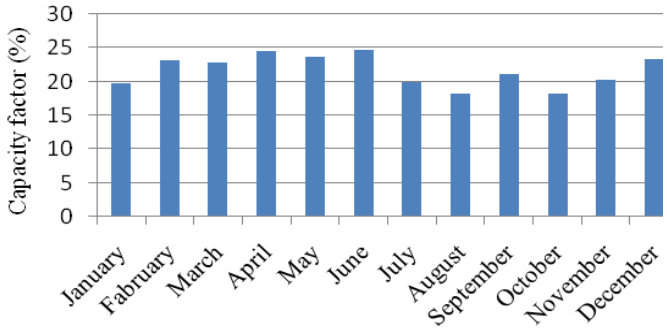

Fig. 10. Capacity factor of the wind turbine

4. Solar photovoltaic energy estimation model

The photovoltaic (PV) subsystem is composed of 400 m² (reserved area) photovoltaic panels interconnected to the fixed DC bus through (DC/DC) boost converters.

4.1 Solar panels installation of the PV station

First, the solar panel size is set at 1.5 m². The proposed solar panel is rated at 200 W_p for an irradiance of 1 kW/m² at 25°C. Moreover, the photovoltaic system will operate with a fixed inclination and an optimal slope throughout the year. We need to correct the solar radiation on a horizontal surface. The solar radiation on a tilted surface [16] is given by

$$\underline{G_T} = \underline{G_H} \cdot k_1 \cdot \frac{\cos(\theta - \beta_s - \delta)}{\cos(\theta - \delta)} \tag{15}$$

where $\underline{G_T}$ = monthly average value of solar radiation on a tilted surface; $\underline{G_H}$ = monthly average value of solar radiation on a horizontal surface; k_1 = radiation correction factor fixed to 0.86; θ = latitude; δ = solar declination and β_s is the tilt angle.

With fixed slope systems, a slope roughly equal to the latitude will typically maximize the annual PV energy production. Therefore, the tilt optimum angle is taken as $\theta = \beta_s = 33.9°$. In fact, the monthly average solar radiation on a horizontal and a tilted surface is given in Fig. 11. We note that the solar radiation on a tilted surface is higher and important especially during the period of October–March and exceeds 3 kWh/m²/d. To avoid shading [19], the spacing p between panels is given by

$$p = \left(\frac{\sin(\beta)}{\tan(\theta_s)} + \cos(\beta) \right) \cdot b_l \tag{16}$$

where θ_s is the shading angle, β_s is the slope angle and b_l is the solar panel length.

Therefore, the spacing p is fixed at 3m. In fact, in the reserved area we can install 154 solar panels.

There are some new PV architecture have recently proposed with some positive and some negative aspects in order to reduce the losses [20,21]. For a case study, Fig. 12 shows the scheme of the PV generating subsystem with two boost choppers. In fact, the PV subsystem is divided into two groups of 77 panels and each group generates a load current of 53.27 A at a voltage of 289.3 V. This architecture offers the advantage of providing less losses (two boost choppers), but the disadvantage of losing half of the installation if one converter fails. To estimate the energy production of the photovoltaic station, a probabilistic approach will be used.

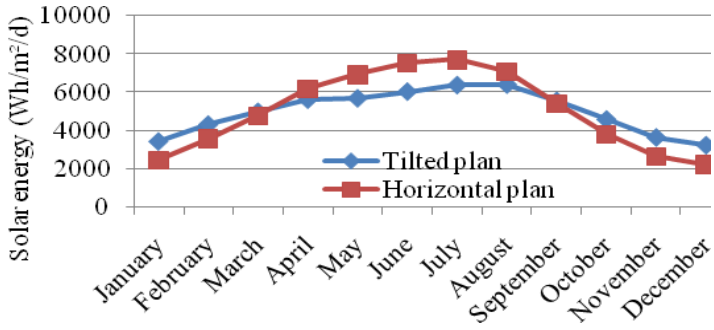

Fig. 11. Solar radiation on a horizontal and a tilted surface

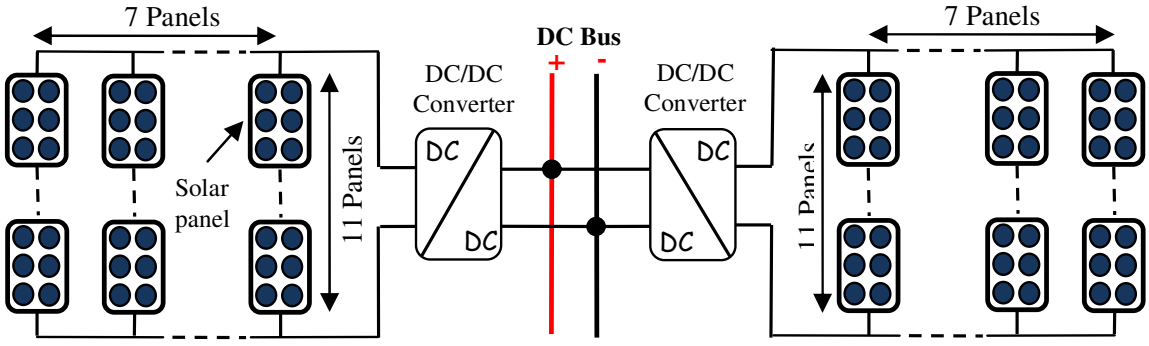

Fig. 12. Photovoltaic subsystem architecture with two boost (DC/DC) converters

4.2 Irradiance probability density functions

In this section, we will use statistical methods to describe random variations of solar radiation [22]. Therefore, the Probability Density Functions are used to fit irradiance distributions. To fit the irradiance data, Weibull, Beta, and Log-normal functions will be used.

4.2.1 Weibull probability density function

The Weibull probability density function is given by

$$f(s)=\frac{k_1}{c_1}\left(\frac{s}{c_1}\right)^{k_1-1}\exp\left\{-\left(\frac{s}{c_1}\right)^{k_1}\right\} \tag{17}$$

where k_1 and c_1 are the Weibull distribution parameters.

4.2.2 Beta probability density function

The Beta probability density function is given by

$$g(s)=\frac{1}{B(\alpha,\beta)}\frac{(s-a)^{\alpha-1}(b-s)^{\beta-1}}{(b-a)^{\alpha+\beta-1}} \tag{18}$$

$$B(\alpha,\beta)=\int_0^1 s^{\alpha-1}\cdot(1-s)^{\beta-1}\,ds \tag{19}$$

where α, β are the Beta distribution parameters and a, b are the lower and upper limits respectively.

4.2.3 Log-normal probability density function

The Log-normal probability density function is given by

$$h(s)=\frac{1}{q\cdot s\cdot\sqrt{2\pi}}\exp\left(-\frac{1}{2}\left(\frac{\ln(s)-m}{q}\right)^2\right) \tag{20}$$

According to the monthly average irradiance data, we generate a typical day for each month. Then this data is fitted to one of the three functions of probability distributions (Weibull, Beta, and Log-normal). Therefore, the PDFs are used to calculate the energy production of the photovoltaic station. Fig. 13 presents the probability density functions superimposed with the observed occurrence frequencies of the studied site for a typical day in the month of August.

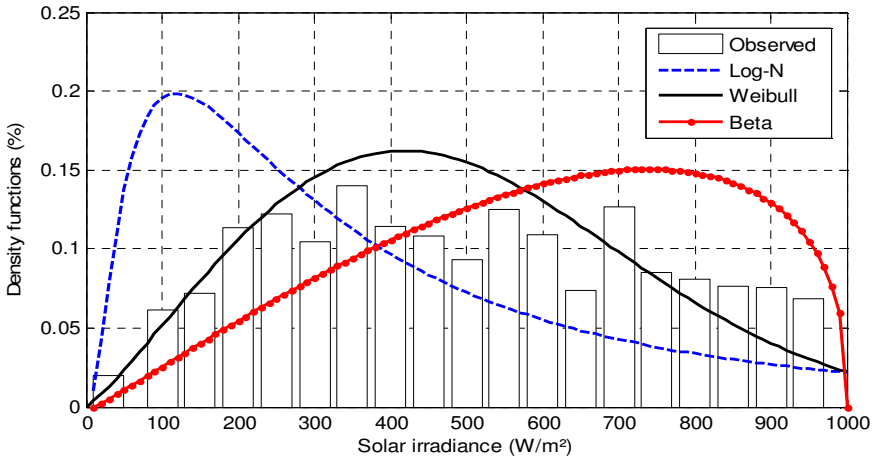

Fig. 13. Weibull, Beta, Log-normal distributions and observed distribution_August

In order to select the best fitted distribution, the Kolmogorov-Smirnov test is used. The K-S test compares the observed cumulative distribution function with the theoretical cumulative distribution function. So, the three distribution functions are tested for the best fit. The K-S tests results for August show that the Weibull distribution is the best fit compared to the Beta and Log-normal distributions. Fig. 14 shows the Weibull distribution and the observed cumulative distribution.

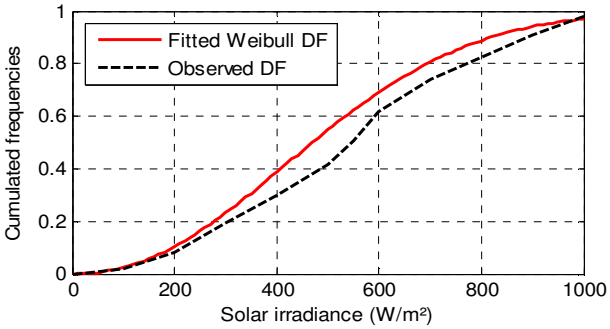

Fig. 14. Weibull and observed cumulative distributions_August

4.3 Solar photovoltaic power

In this paragraph, photovoltaic power from the PV station is investigated in order to estimate the energy production using PDF. Hence, the PV panel output depends on the incident radiation and the cell temperature [16,19]. Including real panels' losses, the output power of the proposed solar panel is calculated by

$$P_{PV} = Y_{PV} \cdot f_{PV}\left(\frac{G_T}{G_{T,STC}}\right) \cdot \left[1 + \alpha_P\left(T_c - T_{c,STC}\right)\right] \tag{21}$$

where Y_{PV} is the rated power output of the PV panel under standard test conditions, f_{PV} is the PV derating factor that shows wiring losses, shading and aging of the panels, G_T is the solar radiation on tilted surface, $G_{T,STC}$ is the radiation at standard test conditions, α_p is the temperature coefficient of power, $T_{c,STC}$ is the PV cell temperature under standard test conditions and T_c is the PV cell temperature.

Therefore, the average photovoltaic power from the PV station is the power produced at each irradiance level under reels conditions (Eq. (21)) multiplied by the Weibull PDF of the irradiance. The average power is given by

$$\overline{P_{PV}} = \int P_{PV}\left(G_T\right) \cdot f\left(G_T\right) \cdot dG_T \tag{22}$$

Then, the monthly average photovoltaic energy is obtained by multiplying the average power by the number of hours. Taking into consideration all of this data and using PDF, the estimated monthly average electricity production from the photovoltaic subsystem is given in Fig. 15. We note here that the annual energy production from the PV station is around 43.93 MWh.

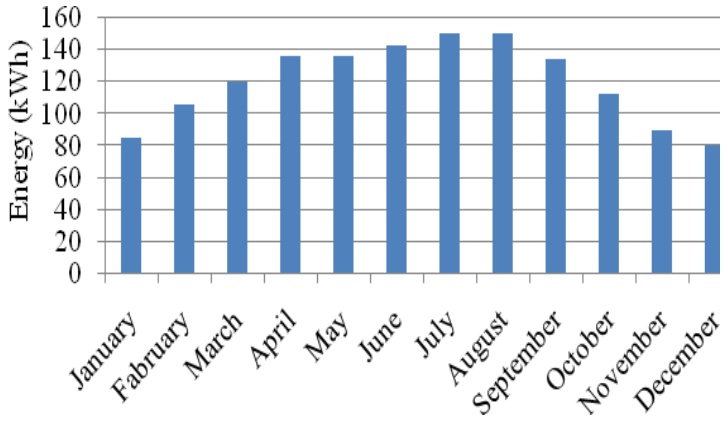

Fig. 15. Photovoltaic energy production using Weibull PDF

4.4 Choppers losses models

The photovoltaic subsystem is composed of 154 PV panels interconnected to a DC bus through two boost (DC/DC) choppers. To estimate electricity at the DC bus, we introduce the conduction and switching losses involved in the (DC/DC) converters [23,24]. The chopper loss model is investigated in WT subsystem section 3.4. In order to evaluate the power loss involved in the boost converters, switching and conduction losses of the IGBT and the diode are computed. Hence, the estimated total power loss of the proposed PV subsystem is 266 W. Fig. 16 shows the estimated monthly average energy production in the DC bus with the global losses integration obtained from the proposed PV subsystem. The monthly average energy production from the PV station is 117 kWh. The PV energy in the DC-bus is decreased by 3% compared to the estimated PV energy with only panels' losses.

Alberto Dolara et al. [25] showed that the effects of module temperature, surface reflectivity, wiring losses, and inverter–transformer efficiency (BOS) can be summarized synthetically in terms of system PR in the case of a photovoltaic (PV) tracking system in Tuscania, Italy. PR is a dimensionless index, which evaluates the net daily/monthly/annual output energy from a PV array under real working conditions with respect to the theoretical system input energy. In [25], the annual PR of a PV plant is about 81% (based on experimental results). In our case, the annual PR of the PV station is about 77.4%. The obtained results show that this methodology resulted in good performance.

Similar to the wind turbine capacity factor, Fig. 17 presents the estimated monthly average capacity factor of the photovoltaic subsystem. It is clear that in the Djerba region the photovoltaic capacity factor varies from 0.10 (winter period) to 0.20 (summer period).

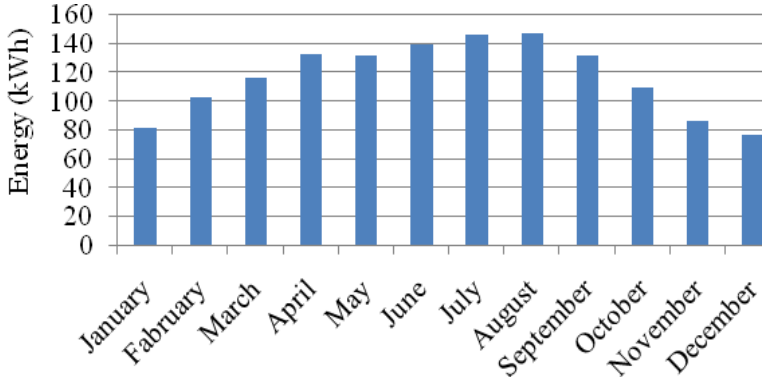

Fig. 16. Photovoltaic energy production including (DC/DC) converters losses

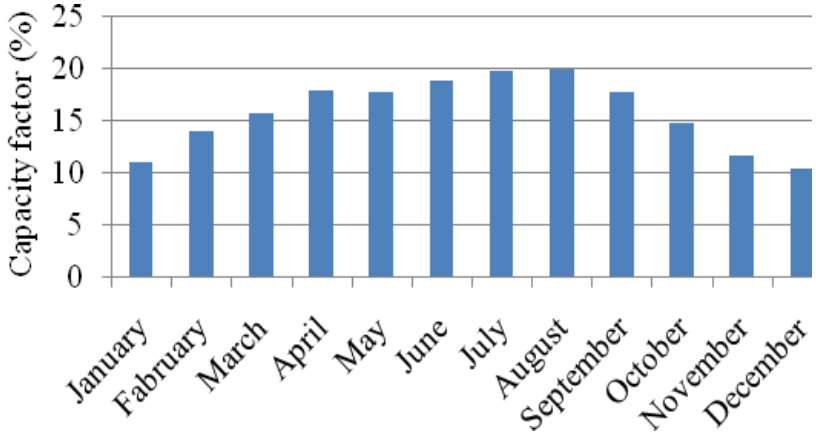

Fig. 17. Capacity factor of the photovoltaic station

5. Hybrid wind-photovoltaic energy

In this paper, a probabilistic approach is used to estimate energy production of the hybrid wind-photovoltaic system. The hybrid system is intended to be used in High Environmental Quality (HEQ) hotels located in Djerba. Indeed, Hybrid energy estimation using PDF (Weibull, Beta, and Log-normal) is presented. The DC bus collects the total energy with the global loss integration involved in the hybrid mini-grid (WT-PV). We give in Fig. 18 the hybrid electrical energy in the DC bus on a large-scale time with the integration of all losses. In the studied site, monthly average hybrid energy varies between 130 kWh to 190 kWh and the annual energy production is around 61.84 MWh. Hence, the hybrid system (PV/Wind) presents an important solution to southern Tunisia for increasing energy needs. The prediction of the hybrid energy with the probability density functions can be generated at any time of the day.

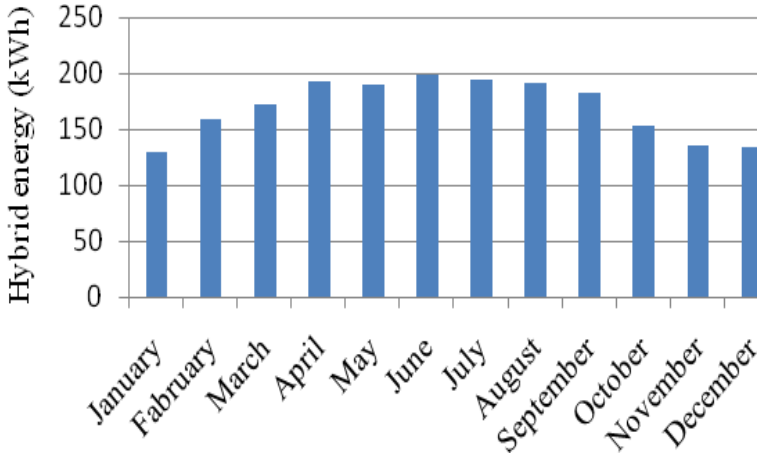

Fig. 18. Hybrid energy production in the DC bus using Statistical Distributions (PDF) and with the global losses integration

6. Conclusion

In this paper the authors have used the statistical distributions to estimate on large-scale time the hybrid energy (photovoltaic and wind) production in southern Tunisia. Geographic and climatic conditions about southern Tunisia were used. An accurate monthly average

hybrid energy estimation taking into consideration all characteristics of the location and using the probability density functions (Weibull, Beta, Log-normal) was presented. The evaluation for hybrid energy production estimation in the DC bus has been investigated with the integration of converters losses. Also, capacity factors of the wind turbine and photovoltaic station were computed. The obtained results show that the integration of converters losses and using statistical distributions models leads to a better energy estimation. It has been shown that the global losses integration is important for accurate hybrid wind turbine-photovoltaic energy estimation and to know how much electrical energy can be extracted. In fact, in southern Tunisia, estimated hybrid energy is important for hotels to supplement the electricity demand.

Acknowledgment

This work was supported by the Tunisian Ministry of High Education and Research under Grant LSE-ENIT – LR 11ES15.

References

[1] E. Akyuz, Z. Oktay, I. Dincer, Performance investigation of hydrogen production from a hybrid wind-PV system, Int. J. Hydrog. Energy. 37 (2012) 16623–16630.

[2] M.H. Nehrir, C. Wang, K. Strunz, H. Aki, R. Ramakumar, J. Bing, Z. Miao, and Z. Salameh, A review of hybrid Renewable/Alternative energy systems for electric power generation: configurations, control, and applications, IEEE Trans. Sustain. Energy. 2 (2011) 392–403.

[3] S.B. Skretas, D.P. Papadopoulos, Efficient design and simulation of an expandable hybrid (wind–photovoltaic) power system with MPPT and inverter input voltage regulation features in compliance with electric grid requirements, Electr. Power Syst. Res. 79 (2009) 1271–1285.

[4] L. Sonia, Z. Dario, Hybrid renewable energy-fuel cell system: Design and performance evaluation, Electr. Power Syst. Res. 79 (2009) 316–324.

[5] O. Ekren, BY. Ekren, B. Ozerdem, Break-even analysis and size optimization of a PV/wind hybrid energy conversion system with battery storage – A case study, Appl. Energy. 86 (2009) 1043–1054.

[6] L. Liu, Z. Wang, The development and application practice of wind–solar energy hybrid generation systems in China, Renew. Sust. Energy Rev. 13 (2009) 1504–1512.

[7] M. Dali, J. Belhadj, X. Roboam, Hybrid solar wind system with battery storage operating in grid-connected and standalone mode: - control and energy management – experimental investigation, Energy. 35 (2010) 2587–2595.

[8] D.V. Brian, A.N. Byron, Analysis of off-grid hybrid wind turbine/solar PV water pumping systems, Sol. Energy. 86 (2012) 1197–1207.

[9] C. Koroneos, A. Dompros, G. Roumbas, Renewable energy driven desalination systems modeling, J. Clean. Prod. 15 (2007) 449–464.

[10] B.S. Borowy, Z.M. Salameh, Methodology for optimally sizing the combination of a battery bank and PV array in a Wind/PV hybrid system. IEEE Trans. Energy Convers. 11 (1996) 367–375.

[11] H. Cherif, J. Belhadj, Large-scale time evaluation for energy estimation of stand-alone hybrid photovoltaic-wind system feeding a reverse osmosis desalination unit, Energy. 36 (2011) 6058–6067.

[12] T.P. Chang, Performance comparison of six numerical methods in estimating Weibull parameters for wind energy application, Appl. Energy. 88 (2011) 272–282.

[13] A.N. Celik, Energy output estimation for small-scale wind power generators using Weibull-representative wind data, J. Wind Eng. Ind. Aerod. 91 (2003) 693–707.

[14] I.Y.F. Lun, J.C. Lam, A study of Weibull parameters using log-term wind observations, Renew. Energy. 20 (2000) 145–153.

[15] C. Novoa, T. Jin, Reliability centered planning for distributed generation considering wind power volatility, Electr. Power Syst. Res. 81 (2011) 1654–1661.

[16] H. Cherif, J. Belhadj, Methodology for accurate energy production estimation of photovoltaic power generation station, IEEE International Mediterranean Electrotechnical Conference,Tunisia. (2012) 561–566.

[17] M. Dali, J. Belhadj, X. Roboam, Control and energy management of a wind-photovoltaic hybrid system, 12th European Conference on Power Electronics and Applications, Denmark. (2007).

[18] Z.M. Salameh, I. Safari, The effect of the windmill's parameters on the capacity factor, IEEE Trans. Energy Convers. 10 (1995) 747–751.

[19] K. Soteris, Solar energy engineering: processes and systems, 1st ed, Burlington, 2009.

[20] F. Foiadelli, S. Leva, D. Zaninelli, PQ and protection system analysis of a new topology for grid connected PV Plant, International Conference on Clean Electrical Power, (2011) 243-248.

[21] M. Brenna, R. Faranda, S. Leva, Dynamic Analysis of a new network topology for high power grid connected PV systems, IEEE Power and Energy Society General Meeting, (2010).

[22] Z.M. Salameh, B.S. Borowy, A.R.A. Amin, Photovoltaic module-site matching based on the capacity factors, IEEE Trans. Energy Convers. 10 (1995) 326–332.

[23] G.R. Walker, P.C. Sernia, Cascaded DC-DC converter connection of photovoltaic modules, IEEE Trans. Power Electron. 19 (2004) 1130–1139.

[24] G. Graditi, D. Colonnese, N. Femia, Efficiency and reliability comparison of DC-DC converters for single phase grid connected photovoltaic inverters, IEEE International Symposium on Power Electronics Electrical Drives Automation and Motion. (2010) 140–147.

[25] A. Dolara, F. Grimaccia, S. Leva, M. Mussetta, R. Faranda, M. Gualdoni, Performance Analysis of a single-Axis Tracking PV System, IEEE J. Photovolt. 2 (2012), 524-531.